Harmonic generation of Li atoms in one- and two-photon Rabi-flopping regimes

K. Nasiri Avanaki, Dmitry A. Telnov, and Shih-I Chu

Phys. Rev. A **94**, 053410 — Published 10 November 2016

DOI: 10.1103/PhysRevA.94.053410

Harmonic generation of Li atoms in one- and two-photon Rabi-flopping regimes

K. Nasiri Avanaki,[1,*] Dmitry A. Telnov,[2,†] and Shih-I Chu[1,3,‡]

[1] *Department of Chemistry, University of Kansas, Lawrence, Kansas 66045, USA*
[2] *Department of Physics, St. Petersburg State University, 7-9 Universitetskaya nab., St. Petersburg 199034, Russia*
[3] *Center for Quantum Science and Engineering, Department of Physics, National Taiwan University, Taipei 10617, Taiwan*

We present a comprehensive theoretical and computational study on harmonic generation (HG) of Li atoms in one- and two-photon Rabi-flopping regimes where the population transfer from the ground $2s$ state to the excited $2p$, $3s$, and $3d$ states is substantial. Our all-electron approach is based on the time-dependent density-functional theory and takes into account polarization of the core and dynamic response of the electrons to the laser field. We show that the population oscillations in the time domain with the Rabi frequency Ω are reflected in the fine structure of the HG spectra in the frequency domain on the scale of 2Ω. Our results also manifest that even finer structures of the harmonic peaks on the smaller frequency scale originate from the pulse-shape-related interference effects. These features are clearly seen in one-photon Rabi-flopping regime between the $2s$ and $2p$ states. The pattern in the HG spectra becomes more complex in the two-photon Rabi-flopping regime involving $3s$ and $3d$ states. Our findings can be used for developing coherent control methods for HG in the Rabi-flopping regime.

PACS numbers: 42.65.Ky,42.50.Hz,32.80.Rm

I. INTRODUCTION

High-order-harmonic generation (HHG) is a fundamental atomic and molecular process in strong laser fields that continues attracting much interest in recent years both experimentally and theoretically [1]. With tunable long-wavelength lasers available, sufficiently high intensities without saturation of ionization can be used for probing both valence and core electrons. HHG processes have a capability of imaging of atomic and molecular structures with high resolution in spatial and temporal domains [2, 3]. The multielectron structural information can be retrieved by means of the HHG interferometry which is established as an effective approach to resolving multielectron dynamics. With laser pulses as short as a few femtoseconds, HHG spectroscopy can also become a possible tool for probing chemical reactions on a femtosecond time scale. Recently the emphasis is more and more shifted from observation of atoms and molecules interacting with laser fields towards their control. Coherent control of photon emission [4] and transient absorption [5] are promising directions in further advancements of ultrafast laser spectroscopy and other related applications.

Since the pioneering work of Rabi [6], coherent population transfer among different energy states has been a powerful technique in controlling quantum systems [7, 8]. In a two-level atomic system interacting with a resonant radiation field, the dynamics of the electronic population presents well-known periodic Rabi oscillations. The phase of Rabi oscillations is associated with the so-called "pulse area". When the latter reaches the value of π (π pulse), the population transfer between the two quantum states is complete. Rabi oscillations play an important role in measuring the pulse area and excited-state population. This is directly incorporated with the pulse duration, intensity, detuning from resonance, and the transition dipole moment. Robust coherent control methods based on the concept of Rabi oscillations are utilized in various recent applications such as ultrafast manipulation of Rydberg states [9–11], quantum information processing [12], ensembles of cold atoms [13–15] etc.

Rabi flopping in multiphoton regime also became feasible with advancements in laser technology and pulse shaping techniques [16–18]. However, this regime requires stronger radiation fields resulting in sloppy population transfer to the target state. The process may become out of control when large a.c. Stark shifts detune the system from the resonance [19]. It should be noted that the origin and dynamics of the population transfer and oscillations are qualitatively different for weak and strong radiation fields [20, 21]. In the one-photon transition, the underlying mechanism of population oscillations is different from that in the two-photon transition since in the latter case the resonant intermediate states are affected. For the same pulse area, complications get more serious as the length of the pulse decreases and the peak intensity becomes higher.

Alkali atoms are of particular interest in both experimental and theoretical studies of light-matter interaction. For the theoretical description, it is important that alkali atoms have a single electron outside the closed shell and can be quite accurately represented by single-active-electron (SAE) models [22, 23]. A recent theoretical work [23] revealed signatures of the carrier-wave Rabi flopping (CWRF) in the harmonic generation spectra of potas-

* nasiri@ku.edu
† d.telnov@spbu.ru
‡ sichu@ku.edu

sium atoms. The CWRF regime [24] is reached when the Rabi frequency becomes comparable with the carrier frequency and characterized by breakdown of the pulse area theorem. In Ref. [23], it was found that the third harmonic in the harmonic generation spectra of K atoms exhibits a complex structure in the CWRF regime. Previously, a similar pattern was reported for the third harmonic generated in narrow-band semiconductors [25].

In the present work, we study the influence of the coherent population transfer in Li atoms on the harmonic generation (HG) spectra in the one- and two-photon Rabi-flopping regimes. Lithium is the lightest alkali atom and has a single s valence electron. On the other hand, it is the simplest atom that exhibits inter-shell electron correlation which can provide a richer testing ground for the theoretical investigation of the interaction of the atom with intense laser fields. While SAE models with the state-of-the-art effective potentials and pseudopotentials may appear very accurate in description of alkali atoms (see, for example, the review article [26] and references therein), they still lack the dynamic multielectron response of the atomic core to the laser fields, which may be significant and affect the outer electron even when the inner electrons are tightly bound. Our theoretical approach goes beyond the SAE approximation and is based on the self-interaction-free time-dependent density-functional theory (TDDFT), which takes into account the electron exchange and correlation through the exchange-correlation functional. Here we use it specifically to study HG of Li atoms driven by strong near-resonant laser fields with realistic parameters such as carrier frequency, peak intensity, and pulse duration that can be used to control the shape and structure of the harmonic peaks. It should be noted that recent TDDFT studies [27–29] revealed failures to describe the Rabi dynamics in two-electron model systems initially in the ground singlet states. Such systems, when treated by TDDFT with adiabatic exchange-correlation functionals (where the potential at any time is a functional of the density at that time), featured incomplete population transfer to the excited states and detuned Rabi oscillations [28]. The system is driven out of resonance when the density changes significantly due to the population transfer to the excited states thus causing a change in the adiabatic Kohn-Sham potential. A conclusion was made [28, 29] that non-adiabaticity of the exchange-correlation functional is crucial to properly capture the physics of Rabi oscillations, and adiabatic functionals would fail to do so. However, as our calculations show, this problem is not severe for the Li atom, which has only one $2s$ electron outside the closed $1s$ shell. The transitions of the valence electron do not affect too much the tightly bound core electrons. That is why the Kohn-Sham mean field experienced by the valence electron does not manifest dramatic changes when the population transfer occurs between the $2s$ and excited states, and the system does not go off the resonance.

For the one-photon Rabi-flopping case, we choose the carrier frequency tuned into the resonance with the transition between the ground $2s$ and the first excited $2p$ states (D-line in the radiation spectrum of Li; the experimental wavelength is 671 nm). The two-photon Rabi-flopping regime can be reached when the carrier frequency of the laser pulse is tuned into the two-photon resonance between the ground $2s$ state and excited $3s$ or $3d$ states. In the HG spectra, we observe characteristic oscillatory structures and explain their relations to the Rabi flopping and pulse-shape-induced interferences. We also discuss systematic shifts of the harmonic peaks when the carrier frequency has a small detuning from the resonance. Our findings can be used for the purpose of coherent control of HG in the Rabi-flopping regime.

The paper is organized as follows. In Sec. II, we provide a detailed description of our theoretical approach in the framework of TDDFT and computational method. In Sec. III, we discuss the results of the calculations and give necessary theoretical explanations. Sec. IV contains concluding remarks.

II. METHOD

We use TDDFT to study harmonic generation of Li atoms driven by strong near-resonant laser fields. The single-particle potential is constructed by means of the Krieger-Li-Iafrate (KLI) procedure [30] with self-interaction correction (SIC) extended to the time-dependent (TD) problems [31]. For the TD-KLI-SIC procedure [31] adopted here, we extend Perdew and Zunger's SIC form [32] to the time domain. It has been shown [31] that the TDKLI procedure [33] can be simplified considerably without the need of using the nonlocal Hartree-Fock energy functional, in the construction of the time-dependent optimized effective potential. Thus the TD-KLI-SIC procedure [31] is computationally more efficient and yet maintains high accuracy in the calculation of the ground state energies, ionization potentials, excited autoionizing resonances [34], as well as multiphoton ionization dynamics [31, 35]. Within the adiabatic approximation, well justified in the case of low-frequency laser fields [36], the TD-KLI-SIC single-particle potential can be expressed as follows:

$$V^{\rm s}_\sigma(\boldsymbol{r},t) = \sum_{j=1}^{N_\sigma} \frac{\rho_{j\sigma}(\boldsymbol{r},t)}{\rho_\sigma(\boldsymbol{r},t)} \left[v_{j\sigma}(\boldsymbol{r},t) + \bar{V}^{\rm s}_{\sigma j} - \bar{v}_{j\sigma} \right]. \quad (1)$$

Here indices j and σ enumerate spin-orbitals (σ corresponds to the spin projection, N_σ is the total number of electrons with the spin σ); $\rho_{j\sigma}$ and ρ_σ are the spin-orbital density and the total spin-density, respectively:

$$\rho_{j\sigma}(\boldsymbol{r},t) = |\psi_{j\sigma}(\boldsymbol{r},t)|^2,$$
$$\rho_\sigma(\boldsymbol{r},t) = \sum_{j=1}^{N_\sigma} \rho_{j\sigma}(\boldsymbol{r},t) \quad (2)$$

($\psi_{j\sigma}(\boldsymbol{r},t)$ is the Kohn-Sham spin-orbital). The orbital-dependent potential $v_{j\sigma}(\boldsymbol{r},t)$ includes the Hartree and exchange-correlation parts as well as self-interaction corrections. The mean values $\bar{V}^{\rm s}_{\sigma j}$, $\bar{v}_{j\sigma}$ are calculated with the spin-densities $\rho_{j\sigma}(\boldsymbol{r},t)$:

$$\bar{V}^{\rm s}_{\sigma j} = \int d^3r \rho_{j\sigma}(\boldsymbol{r},t) V^{\rm s}_{\sigma}(\boldsymbol{r},t),$$
$$\bar{v}_{j\sigma} = \int d^3r \rho_{j\sigma}(\boldsymbol{r},t) v_{j\sigma}(\boldsymbol{r},t). \quad (3)$$

Eq. (1) defines the potential $V^{\rm s}_{\sigma}(\boldsymbol{r},t)$ up to an arbitrary constant. However, since the exchange-correlation potential vanishes at infinity in the space domain, its expectation value with the highest-occupied spin-orbital $\psi_{m\sigma}(\boldsymbol{r},t)$ must be equal to that of the orbital-dependent potential $v_{m\sigma}(\boldsymbol{r},t)$ [30]:

$$\bar{V}^{\rm s}_{\sigma m} = \bar{v}_{m\sigma}. \quad (4)$$

The constraint (4) makes the potential (1) unique, and all unknown constants $\bar{V}^{\rm s}_{\sigma j}$ ($j<m$) can be obtained solving a set of linear equations [30].

For Li atoms, the procedure is particularly straightforward since N_σ does not exceed 2. For the open-shell Li atom (the electronic structure $1s^22s$), the TD-KLI-SIC potential is spin-dependent and can be explicitly written as follows, for the spin up ($\uparrow$) and spin down ($\downarrow$), respectively [37]:

$$V^{\rm s}_{\uparrow}(\boldsymbol{r},t) = \frac{\rho_{1\uparrow}(\boldsymbol{r},t)}{\rho_{\uparrow}(\boldsymbol{r},t)}\Big\{ v_{1\uparrow}(\boldsymbol{r},t) + \left[\int d^3r \frac{\rho_{2\uparrow}(\boldsymbol{r},t)\rho_{1\uparrow}(\boldsymbol{r},t)}{\rho_{\uparrow}(\boldsymbol{r},t)}\right]^{-1} \times \int d^3r \frac{\rho_{2\uparrow}(\boldsymbol{r},t)\rho_{1\uparrow}(\boldsymbol{r},t)}{\rho_{\uparrow}(\boldsymbol{r},t))}[v_{2\uparrow}(\boldsymbol{r},t) - v_{1\uparrow}(\boldsymbol{r},t)]\Big\} + \frac{\rho_{2\uparrow}(\boldsymbol{r},t)}{\rho_{\uparrow}(\boldsymbol{r},t)} v_{2\uparrow}(\boldsymbol{r},t), \quad (5)$$

$$V^{\rm s}_{\downarrow}(\boldsymbol{r},t) = v_{1\downarrow}(\boldsymbol{r},t). \quad (6)$$

For the orbital-dependent potentials $v_{j\sigma}(\boldsymbol{r},t)$, we use the exchange-only approximation in the local spin-density (LSD) form, and include Perdew-Zunger [32] self-interaction corrections:

$$v_{j\sigma}(\boldsymbol{r},t) = v_{\rm H}[\rho_\uparrow+\rho_\downarrow](\boldsymbol{r},t) + v^{\rm LSD}_{\rm x}[\rho_\sigma](\boldsymbol{r},t) - v_{\rm H}[\rho_{j\sigma}](\boldsymbol{r},t) - v^{\rm LSD}_{\rm x}[\rho_{j\sigma}](\boldsymbol{r},t) \quad (7)$$

where $v_{\rm H}[\rho](\boldsymbol{r},t)$ and $v^{\rm LSD}_{\rm x}[\rho](\boldsymbol{r},t)$ are the Hartree and LSD exchange potentials, respectively:

$$v_{\rm H}[\rho](\boldsymbol{r},t) = \int d^3r' \frac{\rho(\boldsymbol{r},t)}{|\boldsymbol{r}-\boldsymbol{r}'|},$$
$$v^{\rm LSD}_{\rm x}[\rho](\boldsymbol{r},t) = -\left[\frac{6}{\pi}\rho(\boldsymbol{r},t)\right]^{1/3}. \quad (8)$$

The spin-orbital energies computed by the time-independent DFT using these potentials are listed in Table I. The highest-occupied orbital energy is in a good agreement with the experimental data for the ionization potential [38]. In Table II, we list the one-electron excitation energies ($2s \to nl$) calculated as differences of the corresponding eigenvalues of the time-independent DFT Hamiltonian. For comparison, experimental excitation energies are also shown. As one can see, the agreement is fairly good (within 2%). Of course, the differences of the Kohn-Sham orbital energies are only a zero-order approximation to the actual excitation energies of the multielectron atom. A better approximation, including the dynamical exchange-correlation effects, can be obtained in the framework of the linear-response TDDFT [39, 40]. For the Li atom, however, the Kohn-Sham level of accuracy is quite good and sufficient to determine the laser frequencies for near-resonant excitations. The same is true for the transition dipole matrix elements calculated between the one-electron Kohn-Sham states with the principal quantum numbers $n=2$ and $n=3$ and listed in Table III. Accuracy of these matrix elements is important for correct description of the excitation dynamics in near-resonant laser fields. As one can see, the quality of the calculated transition dipoles is rather good even on the one-electron Kohn-Sham level; they agree well with the matrix elements obtained by the precision linearized coupled-cluster method [41].

TABLE I. Absolute values of spin-orbital energies of Li. (A) Present calculations (a.u.). (B) Experimental ionization energy of Li [38] (a.u.).

Spin-orbital	A	B
$1s\uparrow$	1.993	
$1s\downarrow$	2.476	
$2s\uparrow$	0.196	0.198

To obtain the time-dependent electron densities and calculate the harmonic spectra, one has to solve a set of the the time-dependent Kohn-Sham equations for the spin-orbitals $\psi_{j\sigma}(\boldsymbol{r},t)$:

$$i\frac{\partial}{\partial t}\psi_{j\sigma}(\boldsymbol{r},t) = \Big[-\frac{1}{2}\nabla^2 - \frac{Z}{r} + V^{\rm s}_{\sigma}(\boldsymbol{r},t) + v_{\rm ext}(\boldsymbol{r},t)\Big]\psi_{j\sigma}(\boldsymbol{r},t), \quad j=1,...,N_\sigma. \quad (9)$$

Besides the discussed single-particle potential $V^{\rm s}_{\sigma}$, the right-hand side of Eq. (9) contains the Coulomb interaction with the nucleus (Z is the nucleus charge) and interaction with the external laser field $v_{\rm ext}(\boldsymbol{r},t)$. In our calculations we use a linearly polarized laser pulse; the envelope has a sine-squared shape and contains 20 optical cycles (o.c.):

$$v_{\rm ext}(\boldsymbol{r},t) = (\boldsymbol{F}(t)\cdot\boldsymbol{r}), \quad (10)$$
$$\boldsymbol{F}(t) = \boldsymbol{F}_0 \sin^2\frac{\pi t}{T}\sin\omega_0 t, \quad T = \frac{40\pi}{\omega_0}. \quad (11)$$

To solve the set (9), we apply the time-dependent generalized pseudospectral (TDGPS) method which proved

TABLE II. $2s \rightarrow nl$ excitation energies of Li. (A) Present calculations (a.u.). (B) Experimental results [42] (a.u.).

nl	A	B
$2p$	0.0673	0.0679
$3s$	0.1219	0.1240
$3p$	0.1389	0.1409
$3d$	0.1401	0.1425

TABLE III. Transition dipole matrix elements $\langle n'l'0|z|nl0\rangle$ of Li. (A) Present calculations (a.u.). (B) Ref. [41] (a.u.).

Transition	A	B
$2s \rightarrow 2p$	2.38	2.35
$2s \rightarrow 3p$	0.113	0.129
$2p \rightarrow 3s$	1.77	1.72
$2p \rightarrow 3d$	2.33	2.27

accurate and efficient in our previous atomic TDDFT calculations (see, *e. g.*, Refs. [37, 43–45]). For the TDGPS discretization in the present calculations, we use 80 radial and 32 angular grid points, and 4096 time steps per optical cycle. The equations (9) are solved in space within a sphere with the radius 60 a.u.; between 40 a.u. and 60 a.u. we place an absorber. Absorbed parts of the wave packet localized beyond 40 a.u. describe unbound states populated during the ionization process. We note that the absorber is located far enough from the nucleus, so its influence on the excitation and ionization dynamics is negligible. Because of the absorber, the normalization integrals of the spin-orbital densities $\rho_{j\sigma}(\boldsymbol{r},t)$ decrease in time. The ionization probabilities $P_{j\sigma}$ for each spin orbital are determined by the densities calculated after the pulse:

$$P_{j\sigma} = 1 - \int d^3r \rho_{j\sigma}(\boldsymbol{r},T). \tag{12}$$

We note that for the moderate peak intensities used in the calculations (up to 2×10^{12} W/cm^2) only the highest-occupied $2s$ orbital of Li contributes to ionization while the tightly bound inner shell $1s$ electrons do not leave the core. Then the ionization probability of Li $\mathcal{P}$ reads as

$$\mathcal{P} = P_{2\uparrow}. \tag{13}$$

To calculate the HG spectra, we use a semiclassical approach, where the basic expressions come from the classical electrodynamics but the classical quantities such as dipole moment and its acceleration are replaced with the corresponding quantum expectation values. The spectral density of radiation energy can be expressed through the Fourier transforms of the dipole acceleration $\boldsymbol{a}(t)$ or dipole moment $\boldsymbol{d}(t)$ [46]:

$$S(\omega) = \frac{2}{3\pi c^3}|\widetilde{\boldsymbol{a}}(\omega)|^2 = \frac{2\omega^4}{3\pi c^3}|\widetilde{\boldsymbol{d}}(\omega)|^2; \tag{14}$$

$$\widetilde{\boldsymbol{a}}(\omega) = \int_{-\infty}^{\infty} dt\ \boldsymbol{a}(t)\exp(i\omega t), \tag{15}$$

$$\widetilde{\boldsymbol{d}}(\omega) = \int_{-\infty}^{\infty} dt\ \boldsymbol{d}(t)\exp(i\omega t), \tag{16}$$

(c is the speed of light) and the expectation values of the dipole moment and its acceleration are defined as follows:

$$\boldsymbol{d}(t) = \int d^3r\ \boldsymbol{r}\ [\rho_\uparrow(\boldsymbol{r},t) + \rho_\downarrow(\boldsymbol{r},t)]; \tag{17}$$

$$\boldsymbol{a}(t) = -\int d^3r\ [\rho_\uparrow(\boldsymbol{r},t) + \rho_\downarrow(\boldsymbol{r},t)] \times \nabla[-\frac{Z}{r} + v_{\rm ext}(\boldsymbol{r},t)]. \tag{18}$$

They satisfy the same relation as the corresponding classical quantities:

$$\frac{d^2}{dt^2}\boldsymbol{d}(t) = \boldsymbol{a}(t). \tag{19}$$

The expression for $\boldsymbol{a}(t)$ can be derived from that for $\boldsymbol{d}(t)$ with the help of the Ehrenfest theorem. We note that only the nuclear and external field potentials are present in Eq. (18). When multielectron targets are treated exactly, the electron-electron interaction *does not* contribute to the expectation value of the dipole acceleration due to Newton's third law since the electrons are identical and have the same masses and charges. In TDDFT, that means the *exact* exchange-correlation potential (as well as the Hartree potential) does not contribute to the expectation value of acceleration (the zero-force theorem [47]). For approximate exchange-correlation potentials, this is not always true. Consequently, the length and acceleration forms of the HG spectra (14) with the expectation values defined in Eqs. (17) and (18) are not necessarily identical in TDDFT. This is specifically the case for the TD-KLI-SIC approximation, which is known to violate the zero-force theorem [48]. In this study, we adopt the length form of the HG spectra as defined by equations (14), (16), and (17).

III. RESULTS AND DISCUSSION

A. One-photon Rabi flopping

In order to have an efficient control over the coherent population transfer in the one-photon Rabi-flopping regime, we set the carrier wavelength to 676 nm ($\omega_0 =$ 0.0674 a.u.) corresponding to a resonance one-photon transition between the ground $2s$ and the first excited $2p$ states (D line in the radiation spectrum of Li; the experimental wavelength is 671 nm). Several peak intensities in the range 2×10^{11} to 2×10^{12} W/cm^2 have been used

TABLE IV. Ionization probabilities ($\mathcal{P}$), Rabi frequencies (Ω), and pulse areas (Θ) for the resonant 20 o.c. $\sin^2$ laser pulses with the carrier wavelength 676 nm.

Peak intensity (W/cm^2)	$\mathcal{P}$	Ω (a.u.)	Θ/π
2.0×10^{11}	0.019	0.00568	1.69
2.8×10^{11}	0.031	0.00672	2.00
3.0×10^{11}	0.035	0.00696	2.07
3.2×10^{11}	0.038	0.00719	2.13
5.0×10^{11}	0.069	0.00899	2.67
1.0×10^{12}	0.135	0.01271	3.77
1.3×10^{12}	0.170	0.01449	4.30
2.0×10^{12}	0.268	0.01797	5.33

in the calculations. Since the excitation dynamics in the resonant field is closely related to the Rabi oscillations and Rabi flopping, let us introduce the Rabi frequency and pulse area. The Rabi frequency Ω is defined as a product of the peak value of the laser electric field F_0 and transition dipole D between the resonant atomic states:

$$\Omega = F_0 D. \tag{20}$$

Then the pulse area Θ is a product of the Rabi frequency Ω and the full width at the half maximum (FWHM) of the laser pulse τ [for the $\sin^2$ pulse, the latter is just one half of the total pulse duration T, see Eq. (11)]:

$$\Theta = \Omega\tau. \tag{21}$$

In the Rabi-flopping regime, the population inversion after the pulse occurs if the pulse area is equal to an odd integer in units of π. For the simplified two-level system, it corresponds to the total depletion of the initial ground state and full population of the excited state. For more realistic multilevel system, this is not the case because a part of the initial population of the ground state may go to other (non-resonant) excited states. Still, the population of the resonant excited state at the end of the pulse can be very significant. If the pulse area is equal to an even integer in units of π, then the most of the population returns to the initial ground state after the pulse.

In Table IV, we present ionization probabilities, Rabi frequencies, and pulse areas for different peak intensities used in the calculations (our laser pulse always has a $\sin^2$ envelope and duration of 20 o.c.). Note that the Rabi frequency is much less than the laser carrier frequency for all intensities in the range. As one can see, at the highest intensity 2.0×10^{12} W/cm^2 ionization of the Li atom is substantial. Using even higher intensities may result in full ionization on the leading edge of the laser pulse and suppression of harmonic generation. Based on the pulse area calculated according to Eq. (21), one may expect the largest ground state population after the 2π-pulse with the peak intensity 2.8×10^{11} W/cm^2. However, the pulse area analysis is an approximate tool coming from

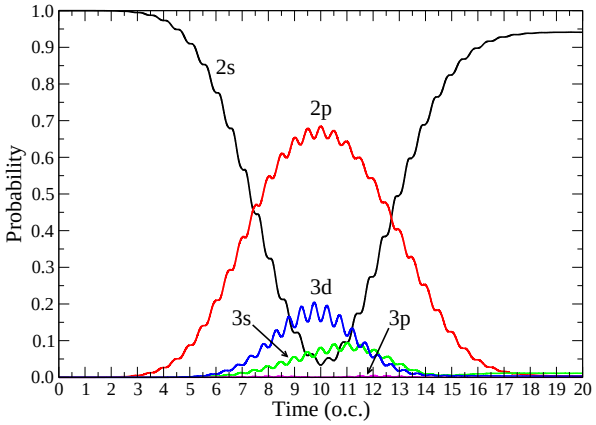

FIG. 1. Time-dependent populations of the ground and several excited states of Li. The laser pulse has a $\sin^2$ shape, duration of 20 o.c., and peak intensity is 3.2×10^{11} W/cm^2. The carrier wavelength 676 nm corresponds to a one-photon resonance between $2s$ and $2p$ states.

the adiabatic two-level system theory. Our numerical calculations show that the largest ground state population after the pulse actually corresponds to the peak intensity 3.2×10^{11} W/cm^2 and pulse area 2.13π. In Fig. 1, the time-dependent populations of the ground ($2s$) and several excited Kohn-Sham states are shown. Similar to the above discussion of the excitation energies and transition dipoles, we should note here that for the Li atom the Kohn-Sham populations are a good approximation for the populations of the ground and singly-excited multielectron states. Besides the resonant $2p$ state, significant populations in the central part of the laser pulse are acquired by the $3s$ and $3d$ states; this happens because these two states are strongly coupled to the $2p$ state (see transition dipoles in Table III), and their excitation energies (Table II) are not far away from the two-photon resonance with the ground state. On the contrary, the population of the $3p$ state is very low (does not exceed 0.005) because this state is not accessible from the $2p$ state through a one-photon process, and transitions from either $2s$, $3s$, and $3d$ states are far from resonance.

The time-dependent dipole moment for the same laser pulse with the peak intensity 3.2×10^{11} W/cm^2 is shown in Fig. 2. The induced dipole moment features a deep low-frequency modulation with the minimum of the envelope at the center of the laser pulse. The modulation frequency is just the Rabi frequency; for this particular laser pulse it is approximately equal to one tenth of the carrier frequency: $\Omega \approx 0.1\omega_0$. The minimum in the induced dipole corresponds to almost full population transfer from the $2s$ state to the $2p$ state at half pulse duration. Note that the dipole moment does not vanish at the end of the laser pulse. It happens because some population still remains in the excited $2p$ state. The frequency of the dipole oscillations at the end of the pulse is not actually the carrier frequency ω_0 of the laser field but the excitation energy of the $2p$ state; the latter, however, is

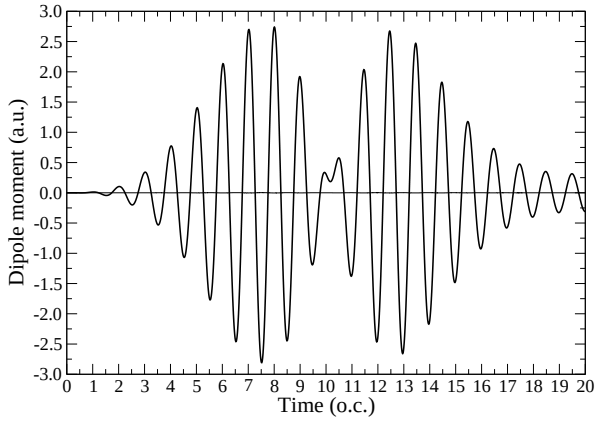

FIG. 2. Time-dependent induced dipole moment in the resonant field. The laser pulse has a $\sin^2$ shape, duration of 20 o.c., and peak intensity is 3.2×10^{11} W/cm^2. The carrier wavelength 676 nm corresponds to a one-photon resonance between $2s$ and $2p$ states.

equal to ω_0 in the resonant field.

To calculate the spectrum of radiation emitted during the interaction with the laser field, one has to perform the Fourier transform of the induced dipole moment [see Eqs. (14) and (16)]. Since we do not propagate the Kohn-Sham orbitals beyond the end of the laser pulse, the temporal integration in Eq. (16) is restricted to the interval from 0 to T, that is the pulse duration. This approach assumes that the dipole moment smoothly goes to zero at both beginning and end of the pulse, otherwise the Fourier transform may contain spurious contributions and noise because of abrupt change of the integrand in Eq. (16). As one can see in Fig. 2, in the case of the resonant (or near-resonant) field, at the end of the pulse the dipole moment still oscillates with a quite large magnitude and does not vanish. To avoid any unwanted effects in the Fourier transform, before taking the integral in Eq. (16), we multiply the dipole moment by the window function, which is equal to unity in the central part of the laser pulse and smoothly goes to zero at both $t = 0$ and $t = T$. In our calculations, we use the following window function $W(t)$:

$$W(t) = \begin{cases} \sin^2\left(\dfrac{\omega_0 t}{8}\right), & 0 \le t < \dfrac{4\pi}{\omega_0}; \\ 1, & \dfrac{4\pi}{\omega_0} \le t < T - \dfrac{4\pi}{\omega_0}; \\ \sin^2\left(\dfrac{\omega_0 (T-t)}{8}\right), & T - \dfrac{4\pi}{\omega_0} \le t \le T. \end{cases} \tag{22}$$

Defined in this way, the function $W(t)$ gradually raises from 0 to 1 during the first two optical cycles, remain equal to unity for the next 16 optical cycles, and gradually decreases to zero during the last two optical cycles.

In Fig. 3, we show the HG spectrum obtained by the Fourier transform with the window function (22) for the same laser pulse with the carrier wavelength 676 nm and peak intensity 3.2×10^{11} W/cm^2. The spectrum consists of distinct odd harmonic peaks manifesting fine oscillatory structures. We note that at the laser wavelength 676 nm the third harmonic already corresponds to the photon energy slightly above the ionization threshold, so all generated harmonics are above-threshold, and their frequency profiles are rather broad. The most prominent feature of the spectrum is an oscillatory structure superimposed onto the conventional harmonic peaks. The spacing between the adjacent maxima of this structure is about $0.2\omega_0$, that is twice the Rabi frequency. The origin of these fine oscillations in the frequency domain can be understood from the analysis of the properties of the induced dipole moment in the time domain, which is strongly affected by the population transfer in the resonant field. In the two-level system, the dipole moment vanishes when does so the population of any of the two states strongly coupled by the field. Although this example is oversimplified, it catches the physics of the process; we can see a deep minimum of the dipole moment induced by the field in the Li atom (Fig. 2) when the $2s$ state is almost depleted. The pattern in Fig. 2 exhibits two well-separated portions shifted from each other by 5 o.c. or half the Rabi period, π/Ω. Then we can represent the whole function $d(t)$ as a sum of left and right contributions:

$$d(t) = d_L(t) + d_R(t) \tag{23}$$

and approximate the right contribution as the left one shifted by π/Ω:

$$d_R(t) = d_L(t - \pi/\Omega). \tag{24}$$

Performing the Fourier transform of $d(t)$, one obtains:

$$\widetilde{d}(\omega) = 2 \exp\left(i\frac{\pi\omega}{2\Omega}\right) \cos\left(\frac{\pi\omega}{2\Omega}\right) \widetilde{d}_L(\omega). \tag{25}$$

The spectral density of emitted radiation energy will manifest an oscillatory structure with the adjacent maxima separated by $\Delta\omega = 2\Omega$:

$$S(\omega) = \frac{8\omega^4}{3\pi c^3} \cos^2\left(\frac{\pi\omega}{2\Omega}\right) |\widetilde{d}_L(\omega)|^2. \tag{26}$$

Although the above analysis is approximate, it reveals the origin of the oscillatory structure in the HG spectrum. This structure appears due to low-frequency modulation of the time-dependent dipole moment. The modulation, in turn, has its origin in the population oscillations with the Rabi frequency. We should note that the modulation affects not only the visible time evolution of the dipole moment (with the carrier frequency ω_0) shown in Fig. 2. Higher harmonics also exhibit such a modulation. We can extract time profiles for higher harmonics performing inverse Fourier transforms on the limited frequency range, corresponding to the specific harmonic. For example, taking the inverse Fourier transform of $\widetilde{d}(\omega)$ restricted to the frequency range $[2.5\omega_0, 3.5\omega_0]$, we obtain the time profile for the third harmonic, and similar for

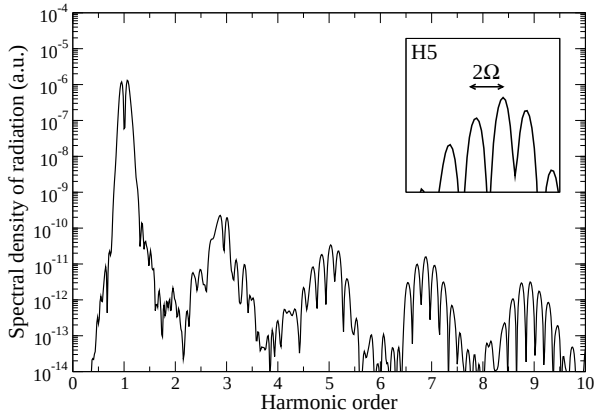

FIG. 3. HG spectrum of Li. The laser pulse has a $\sin^2$ shape, duration of 20 o.c., and peak intensity is 3.2×10^{11} W/cm^2. The carrier wavelength 676 nm corresponds to a one-photon resonance between $2s$ and $2p$ states. The inset shows enlarged structure of the 5th harmonic with the spacing between two adjacent subpeaks equal to 2Ω.

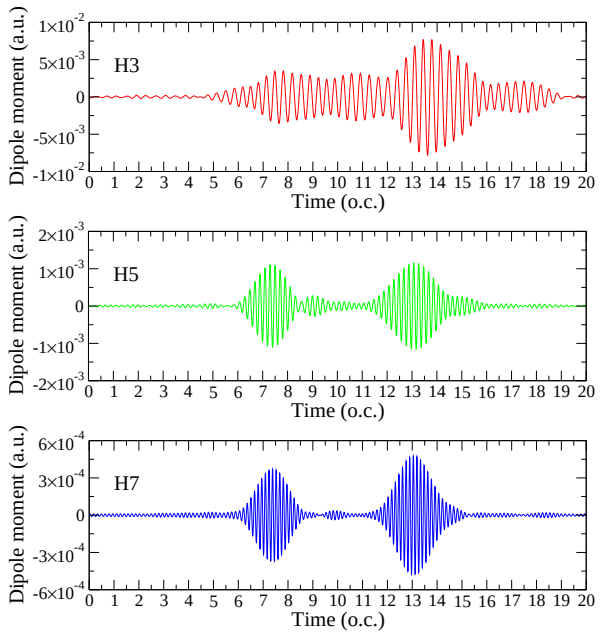

FIG. 4. Time profiles of the 3rd, 5th, and 7th harmonics. The laser pulse has a $\sin^2$ shape, duration of 20 o.c., and peak intensity is 3.2×10^{11} W/cm^2. The carrier wavelength 676 nm corresponds to a one-photon resonance between $2s$ and $2p$ states.

other harmonics. In Fig. 4, the time profiles for the harmonic orders 3, 5, and 7 are shown. As one can see, the 5th and 7th harmonics exhibit a well-pronounced low-frequency modulation similar to that seen in Fig. 2. The time profile for the third harmonic is somewhat different; although the modulation is present, its frequency cannot be easily extracted from the time profile since there is only one dominant contribution from the time interval 13 to 15 o.c. Nonetheless, the third harmonic also exhibits a subpeak structure in the frequency domain (see Fig. 3) with the spacing between the subpeaks approximately equal to 2Ω.

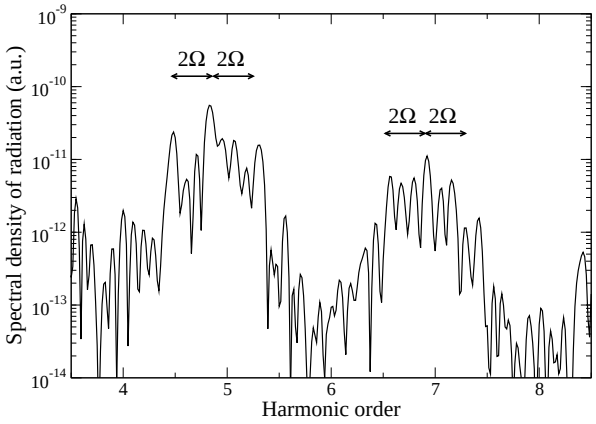

FIG. 5. Fine structures of the 5th and 7th harmonics. The subpeak spacing is less than 2Ω. The laser pulse has a $\sin^2$ shape, duration of 20 o.c., and peak intensity is 1×10^{12} W/cm^2. The carrier wavelength 676 nm corresponds to a one-photon resonance between $2s$ and $2p$ states.

B. Effect of the pulse shape: interference oscillatory structures in HG spectra

At higher peak intensities of the laser pulse, fine oscillatory structures with the subpeak spacing less than 2Ω can be noticed in the harmonic peaks. In Fig. 5, such structures contained within 2Ω frequency intervals are clearly seen in the 5th and 7th harmonics at the peak intensity 1×10^{12} W/cm^2. This phenomenon can be explained by interference of the contributions to the HG spectrum coming from the leading and trailing edges of the laser pulse. As early as in 1984, it was discovered [49] that the spectrum of resonance fluorescence of a two-level system has a multipeak structure. Similar structures were found in the spectra of resonance ionization [50], resonance autoionization [51, 52] and multiphoton above-threshold detachment [53]. In Refs. [52, 53], a concept of adiabatic Floquet states [54, 55] was used to explain the multipeak structures in the spectra. The same approach is applicable for description of the HG spectra.

For the sake of simplicity, let us consider the case when the carrier frequency is tuned into the exact resonance with the transition between the $2s$ and $2p$ states. In this case, the time-dependent wave function can be represented by an equally weighted linear combination of *two* adiabatic Floquet states:

$$\psi = \frac{1}{2}\Big\{ \exp\left[-i\int_0^t \varepsilon_a(\tau)d\tau\right]\psi_a + \exp\left[-i\int_0^t \varepsilon_b(\tau)d\tau\right]\psi_b\Big\}, \tag{27}$$

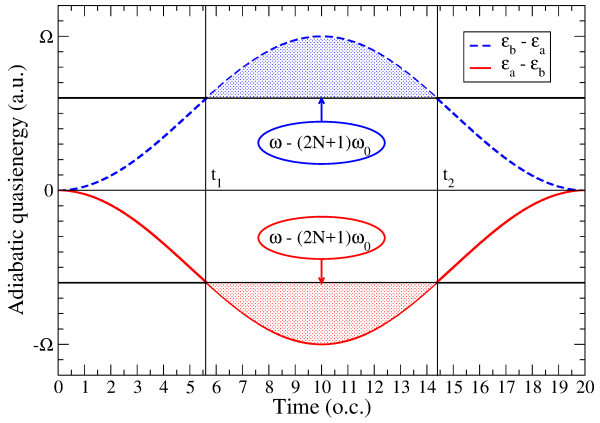

FIG. 6. Adiabatic quasienergies in the resonance field. The time moments t_1 and t_2 denote the saddle points, and the shaded areas represent the phase difference responsible for the interference oscillations.

where ψ_a and ψ_b can be expanded in Fourier series:

$$\psi_a = \sum_n \psi_{a,n} \exp(-in\omega_0 t), \tag{28}$$

$$\psi_b = \sum_n \psi_{b,n} \exp(-in\omega_0 t). \tag{29}$$

The quasienergies ε_a, ε_b and Fourier components $\psi_{a,n}$, $\psi_{b,n}$ depend on time *adiabatically* through the pulse envelope function. In the weak laser field limit, the adiabatic quasienergies ε_a and ε_b become degenerate (and equal to the $2s$ orbital energy), and the wave functions have the following approximate expressions:

$$\psi_a \approx \frac{1}{2}\left[\psi_{2s} + \exp(-i\omega_0 t)\psi_{2p}\right], \tag{30}$$

$$\psi_b \approx \frac{1}{2}\left[\psi_{2s} - \exp(-i\omega_0 t)\psi_{2p}\right], \tag{31}$$

where ψ_{2s} and ψ_{2p} denote unperturbed time-independent $2s$ and $2p$ wave functions, respectively. Then only the $2s$ state is populated at the beginning of the laser pulse ($t = 0$).

With the wave function (27), the expectation value of the induced dipole moment is calculated as follows:

$$\begin{aligned} d(t) = \frac{1}{4}\Big\{ & \langle\psi_a|z|\psi_a\rangle + \langle\psi_b|z|\psi_b\rangle \\ & + \exp\left[i\int_0^t (\varepsilon_a - \varepsilon_b)d\tau\right]\langle\psi_a|z|\psi_b\rangle \\ & + \exp\left[i\int_0^t (\varepsilon_b - \varepsilon_a)d\tau\right]\langle\psi_b|z|\psi_a\rangle\Big\}. \end{aligned} \tag{32}$$

Note that in the resonance field the difference of adiabatic quasienergies is equal to the adiabatic Rabi frequency defined for the the electric field peak value at time t:

$$\varepsilon_b(t) - \varepsilon_a(t) = \Omega(t). \tag{33}$$

Expanding the right-hand side of Eq. (32) in Fourier series, one obtains:

$$\begin{aligned} D(t) = \frac{1}{4}\Big\{ & \sum_n \exp(in\omega_0 t)\left[d_n^{aa} + d_n^{bb}\right] \\ & + \exp\left[i\int_0^t (\varepsilon_a - \varepsilon_b)d\tau\right]\sum_n \exp(in\omega_0 t) d_n^{ab} \\ & + \exp\left[i\int_0^t (\varepsilon_b - \varepsilon_a)d\tau\right]\sum_n \exp(in\omega_0 t)\left[d_{-n}^{ab}\right]^*\Big\} \end{aligned} \tag{34}$$

where

$$d_n^{aa} = \sum_m \langle\psi_{a,m+n}|z|\psi_{a,m}\rangle, \tag{35}$$

$$d_n^{bb} = \sum_m \langle\psi_{b,m+n}|z|\psi_{b,m}\rangle, \tag{36}$$

$$d_n^{ab} = \sum_m \langle\psi_{a,m+n}|z|\psi_{b,m}\rangle. \tag{37}$$

Due to parity restrictions, d_n^{aa}, d_n^{aa}, and d_n^{ab} are non-zero for odd n only.

For the laser field parameters used in the present calculations, the adiabatic Rabi frequency is much less than the carrier frequency at any time: $\Omega(t) \ll \omega_0$. Then the interference oscillatory structure is well localized within a single harmonic frequency profile. For the harmonic order $2n+1$, the time-dependent dipole moment is approximately expressed as

$$\begin{aligned} D_{2n+1}(t) = \frac{1}{4}\Big\{ & \exp[i(2n+1)\omega_0 t]\left[d_{2n+1}^{aa} + d_{2n+1}^{bb}\right] \\ & + \exp\left[i(2n+1)\omega_0 t - i\int_0^t (\varepsilon_b - \varepsilon_a)d\tau\right] d_{2n+1}^{ab} \\ & + \exp\left[i(2n+1)\omega_0 t + i\int_0^t (\varepsilon_b - \varepsilon_a)d\tau\right]\left[d_{-(2n+1)}^{ab}\right]^*\Big\}. \end{aligned} \tag{38}$$

The Fourier transform of Eq. (38) gives the frequency profile of the $(2n+1)$th harmonic. An oscillatory pattern in this profile appears due to the contributions of the last two terms in the right-hand side of Eq. (38). To evaluate these two contributions to the Fourier integral, we apply the saddle-point method. The equations for the saddle points are as follows (ω being the frequency value where the HG spectrum is calculated):

$$\omega = (2n+1)\omega_0 + [\varepsilon_b - \varepsilon_a](t), \tag{39}$$

$$\omega = (2n+1)\omega_0 - [\varepsilon_b - \varepsilon_a](t). \tag{40}$$

Obviously, real-valued t solutions of Eq. (39) exist only if the frequency ω falls into the interval between $(2n+1)\omega_0$ and $(2n+1)\omega_0 + \Omega$. Similarly, real solutions of Eq. (40) exist if the ω value is between $(2n+1)\omega_0 - \Omega$ and $(2n+1)\omega_0$. Since the function $[\varepsilon_b - \varepsilon_a](t)$ is even for symmetric laser pulses, Eqs. (39) and (40) each produce two saddle points, t_1 and $t_2 = -t_1$, as shown in Fig. 6. The contributions from t_1 (leading edge of the laser pulse)

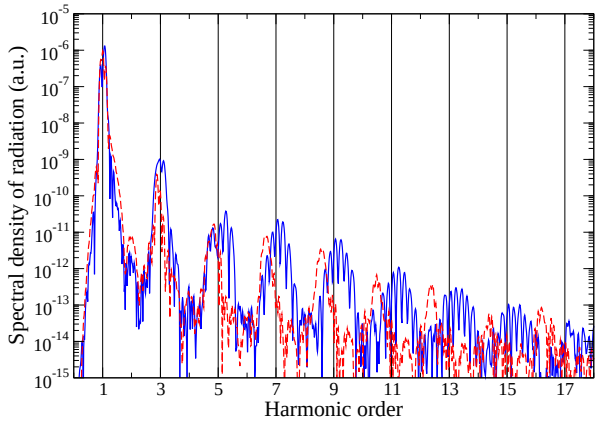

FIG. 7. HG spectra of Li for the driving field wavelength 650 nm (dashed red line) and 700 nm (solid blue line). The laser pulse has a $\sin^2$ shape, duration of 20 o.c., and peak intensity is 3×10^{11} W/cm^2. The 650 nm and 700 nm spectra are red- and blue-shifted, respectively, from the conventional harmonic positions corresponding to odd integer numbers.

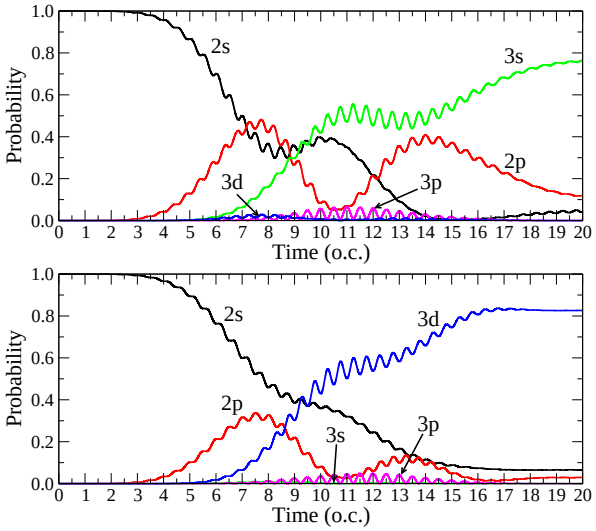

FIG. 8. Time-dependent populations of the ground and several excited states of Li. The laser pulse has a $\sin^2$ shape, duration of 20 o.c., and peak intensity is 5×10^{11} W/cm^2. The carrier wavelength is 730 nm (upper panel) and 640 nm (lower panel).

and t_2 (trailing edge of the laser pulse) interfere resulting in the oscillatory behavior of the Fourier transform as a function of the frequency ω:

$$\widetilde{d}(\omega) \sim d^{ab}_{2n+1}(t_2)\cos\left[\frac{1}{2}\Theta(t_2)\right], \qquad (41)$$

where t_2 is determined by ω according to the equation

$$\omega = (2n+1)\omega_0 + [\varepsilon_b - \varepsilon_a](t_2) \qquad (42)$$

and

$$\widetilde{d}(\omega) \sim \left[d^{ab}_{-(2n+1)}(t_2)\right]^* \cos\left[\frac{1}{2}\Theta(t_2)\right], \qquad (43)$$

where t_2 is determined by the equation

$$\omega = (2n+1)\omega_0 - [\varepsilon_b - \varepsilon_a](t_2). \qquad (44)$$

Eqs. (41) and (43) describe oscillations in the frequency profile of the harmonic on the right and left of the central line $(2n+1)\omega_0$, respectively. The phase difference $\Theta(t_2)$ is given by the shaded areas in Fig. 6 and represents the partial pulse area:

$$\Theta(t_2) = \int_{t_1}^{t_2} dt[\varepsilon_b - \varepsilon_a](t) - (t_2 - t_1)[\varepsilon_b - \varepsilon_a](t_2). \quad (45)$$

The multipeak structure due to interference of the contributions from the leading and trailing edges of the laser pulse is contained within the interval of the width 2Ω and appears on both sides of the central line $(2n+1)\omega_0$. The highest subpeaks of this structure are shifted from the central line by the Rabi frequency Ω corresponding to the peak intensity of the laser pulse. The spectral density of the harmonic may exhibit a multipeak structure due to interference as described above if the peak intensity of the pulse is sufficiently high. For the first interference minimum in the harmonic frequency profile to show up, the pulse area must be greater or equal to π. Since only the central part of the laser pulse (where the field is strong enough) contributes to production of high harmonics, in reality the pulse area should be substantially larger than π to observe this multipeak structure. We should also note that the theoretical description given above is accurate for a two-level system but can be only approximate for real Li atoms. Even in the close vicinity of the $2s-2p$ resonance, population of the other excited states may be significant, especially at high intensities of the laser field, and the resonance approximation involving two adiabatic Floquet states may become invalid.

C. Blue and red shifts of HG spectra near the resonance

In the vicinity of the resonance, the spectrum of emitted radiation is enhanced and dominated by the transition frequency between the $2s$ and $2p$ states, and its harmonics. When the carrier of the driving laser field has a small detuning from the resonance, the spectrum is still dominated by the harmonics of the transition frequency, and not the carrier frequency. Plotted on the scale of the carrier frequency, the harmonic peaks in the spectrum manifest a blue or red shift from odd integers, depending on the sign of the detuning. In Fig. 7, we show the HG spectra for $\sin^2$ laser pulses with the carrier wavelengths 650 nm and 700 nm. For 650 nm, detuning from the resonance (676 nm) is positive (in terms of the frequency), and for 700 nm, detuning is negative. As one can see,

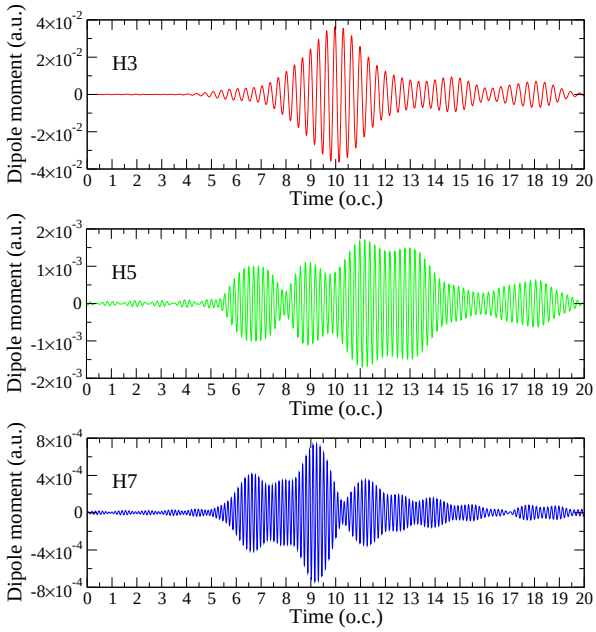

FIG. 9. Time profiles of the 3rd, 5th, and 7th harmonics. The laser pulse has a $\sin^2$ shape, duration of 20 o.c., and peak intensity is 5×10^{11} W/cm^2. The carrier wavelength 730 nm corresponds to a two-photon Rabi-flopping regime between $2s$ and $3s$ states.

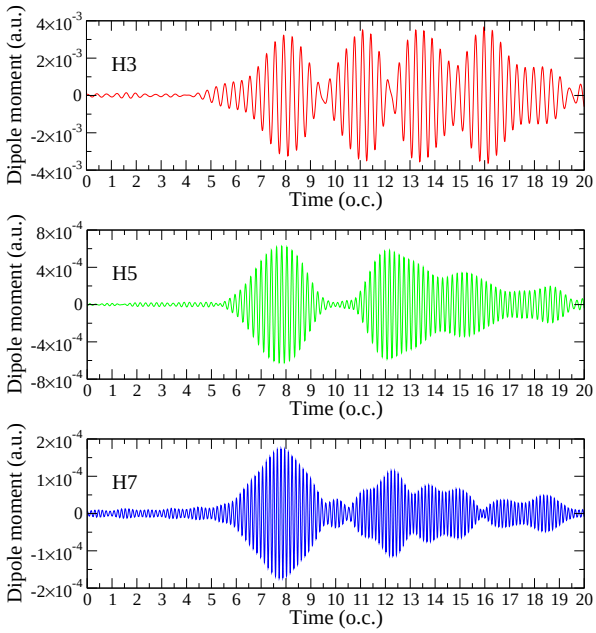

FIG. 10. Time profiles of the 3rd, 5th, and 7th harmonics. The laser pulse has a $\sin^2$ shape, duration of 20 o.c., and peak intensity is 5×10^{11} W/cm^2. The carrier wavelength 640 nm corresponds to a two-photon Rabi-flopping regime between $2s$ and $3d$ states.

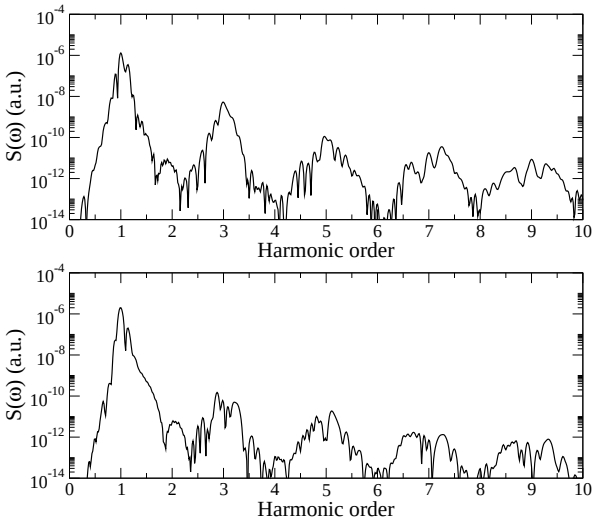

FIG. 11. HG spectra of Li for the driving field wavelengths 730 nm (upper panel) and 640 nm (lower panel), corresponding to two-photon Rabi flopping. The laser pulse has a $\sin^2$ shape, duration of 20 o.c., and peak intensity is 5×10^{11} W/cm^2.

the 650 nm and 700 nm spectra have pronounced red and blue shifts, respectively. The shifts of the harmonic peaks are linearly increasing with the harmonic order. This pattern is well explained if it is understood that the positions of the peaks are determined by odd integers of the transition frequency. Then the very first peak is shifted by the negative value of the resonance detuning δ. For the harmonic of the order $2n+1$, the shift is equal to $-(2n+1)\delta$. We note that the systematic red and blue shifts of the harmonics can only be detected in the close vicinity of the resonance. Far from the resonance, the role of the transition frequency in the radiation spectra is not so important, and the harmonic peaks return to their conventional positions at odd integer multiples of the driving field frequency.

D. Two-photon Rabi flopping

The two-photon Rabi-flopping regime can be reached when the carrier frequency of the laser pulse is tuned into the two-photon resonance between the ground $2s$ state and excited $3s$ or $3d$ states. According to the data in Table II, the corresponding wavelengths must be 748 and 650 nm. However, we have found that larger population transfers to the $3s$ and $3d$ states occur at slightly different carrier wavelengths, 730 and 640 nm, respectively. This may happen due to the interplay between the one-photon $2s-2p$ and two-photon resonance transitions, as well as because of slight difference between the one-electron Kohn-Sham and TDDFT excitation energies. In Fig. 8, we show the time-dependent populations for the peak intensity of the laser pulse 5×10^{11} W/cm^2 and carrier wavelengths 730 and 640 nm. At the end

of the laser pulse, the population inversion is observed, with the largest population in the $3s$ state (730 nm) and $3d$ state (640 nm). In the central part of the pulse, one can see a complex pattern with comparable populations of $2s$, $2p$, and $3s$ states at 730 nm and $2s$, $2p$, and $3d$ states at 640 nm. This population behavior is reflected in a more complex modulation of the dipole moments (see harmonic time profiles in Figs. 9 and 10) and additional fine structure of the harmonics in the frequency domain (Fig. 11) not seen in the case of one-photon Rabi flopping at the same peak intensity. At the carrier wavelength 730 nm, the time profile of the 3rd harmonic has a dominant maximum in the center of the laser pulse, while the time profiles of the 5th and 7th harmonics exhibit several maxima and modulations with the frequency higher than the Rabi frequency for the $2s-2p$ transition (see Fig. 9). Accordingly, in the HG spectrum (Fig. 11, upper panel) the 5th and 7th harmonics have complex multipeak structures while the 3rd harmonic is dominated by a single peak. At the wavelength 640 nm, the pattern is somewhat different. Here the time profile of the 3rd harmonic displays a deep low-frequency modulation with four distinct maxima (Fig. 10). This modulation is reflected in a clear multipeak structure of the 3rd harmonic in the frequency domain (Fig. 11, lower panel). The 5th harmonic in the time domain has two main maxima, corresponding to the modulation with the Rabi frequency (similar to that in the one-photon Rabi-flopping regime, see Fig. 4). In the frequency domain, this harmonic exhibits two distinct peaks separated by 2Ω, although a fine higher-frequency oscillatory structure is also present. Similar structures in the time and frequency domains are also observed in the 7th harmonic.

IV. CONCLUSION

In this paper, we have studied harmonic generation of the lithium atoms in one- and two-photon Rabi-flopping regimes where the population transfer from the ground $2s$ state to the excited $2p$, $3s$, and $3d$ states is substantial. The Li atoms interacting with strong laser fields are described in the framework of the self-interaction-free time-dependent density-functional theory, taking into account dynamic multielectron response to the external field. Using the time-dependent generalized pseudospectral method with sufficient number of spatial grid points and time steps ensures the accuracy and efficiency of the computational procedure.

In the one-photon Rabi-flopping regime, when the carrier frequency of the driving field is tuned in the resonance between $2s$ and $2p$ states, the spectrum of emitted harmonic radiation exhibits a fine oscillatory structure, with the spacing between the adjacent subpeaks equal to twice the Rabi frequency. We have shown that this structure results from the low-frequency modulation of the time-dependent dipole moment. This modulation affects not only the fundamental frequency component of the dipole moment but also the higher frequency Fourier components. The low-frequency modulation of the dipole moment has its origin in the Rabi oscillations of the electronic population between the $2s$ and $2p$ states. Minima in the envelope function of the dipole moment are observed when the $2s$ or $2p$ population becomes extremely small. The number of the minima and their position on the time scale depend on the laser pulse area, that is the peak intensity and pulse duration.

When the peak intensity is increased, the pattern in the harmonic generation spectra becomes more complicated. First, since we study not a two-level system but a realistic multilevel atomic system, population transfer to other excited states becomes more significant with increasing intensity thus disrupting pure two-state Rabi oscillations. Second, the pulse-shape-induced interference effects also become more important at higher intensities. Using the concept of adiabatic Floquet states, we have shown that interference of the contributions to the harmonic generation spectra from the leading and trailing edges of the laser pulse also leads to oscillatory structures of the harmonic peaks but on a smaller frequency scale, well within the double Rabi frequency interval.

Increasing the peak intensity and changing the carrier frequency of the laser field, we can reach the two-photon Rabi-flopping regime. With the electronic structure of Li atoms, detuning the frequency by $\pm 10\%$ off the $2s-2p$ resonance, we can tune into $2s-3s$ or $2s-3d$ two-photon resonances. In this regime, depending on the frequency selected, the population transfer to the $3s$ or $3d$ states may be substantial. In the two-photon $2s-3s$ and $2s-3d$ transitions, the $2p$ energy level plays a role of an intermediate state. Since the detuning from the $2s-2p$ resonance is not very large, population of the $2p$ state may be significant, too. Then in the central part of the laser pulse the population is transferred among three different states ($2s$, $2p$, $3s$ or $2s$, $2p$, $3d$), and all these states may have comparable populations. Such a behavior of the electronic population is reflected in complex modulation patterns of the dipole moment and complex oscillatory structures of the harmonic peaks in the frequency domain.

In conclusion, we should note that the multipeak oscillatory pattern emerging in the harmonic generation spectra in the Rabi-flopping regime is not specific to the lithium atoms only. With appropriate adjustment of the laser pulse parameters, it can also show up in other atomic and molecular targets with a similar structure of electronic energy levels.

ACKNOWLEDGMENTS

This work is partially supported by the Chemical Sciences, Geosciences, and Biosciences Division of the Office of Basic Energy Sciences, U.S. Department of Energy. We also are thankful for the partial support of the Ministry of Science and Technology of Taiwan and National Taiwan University (Grants No.105R891401 and

No. 105R8700-2). D.A.T. acknowledges the partial support from Russian Foundation for Basic Research (Grant No. 16-02-00233).

[1] F. Krausz and M. Ivanov, Reviews of Modern Physics **81**, 163 (2009).

[2] J. Itatani, J. Levesque, D. Zeidler, H. Niikura, H. Ppin, J.-C. Kieffer, P. B. Corkum, and D. M. Villeneuve, Nature **432**, 867 (2004).

[3] O. Smirnova, Y. Mairesse, S. Patchkovskii, N. Dudovich, D. Villeneuve, P. Corkum, and M. Y. Ivanov, Nature **460**, 972 (2009).

[4] M. Chini, X. Wang, Y. Cheng, H. Wang, Y. Wu, E. Cunningham, P.-C. Li, J. Heslar, D. A. Telnov, S.-I. Chu, and Z. Chang, Nat. Photonics **8**, 437 (2014).

[5] M. Chini, X. Wang, Y. Cheng, Y. Wu, D. Zhao, D. A. Telnov, S.-I. Chu, and Z. Chang, Sci. Rep. **3**, 1105 (2013).

[6] I. I. Rabi, Phys. Rev. **51**, 652 (1937).

[7] S. I. Chu, Adv. Chem. Phys. **73**, 739 (1989).

[8] K. Bergmann, H. Theuer, and B. W. Shore, Rev. Mod. Phys. **70**, 1003 (1998).

[9] M. Fushitani, C.-N. Liu, A. Matsuda, T. Endo, Y. Toida, M. Nagasono, T. Togashi, M. Yabashi, T. Ishikawa, Y. Hikosaka, T. Morishita, and A. Hishikawa, Nat. Photon. **10**, 102 (2016).

[10] B. Huber, T. Baluktsian, M. Schlagmüller, A. Kölle, H. Kübler, R. Löw, and T. Pfau, Phys. Rev. Lett. **107**, 243001 (2011).

[11] J. J. Carrera and S. I. Chu, J. Phys. Chem. A **111**, 9320 (2007).

[12] M. Saffman, T. G. Walker, and K. Mølmer, Rev. Mod. Phys. **82**, 2313 (2010).

[13] M. Reetz-Lamour, T. Amthor, J. Deiglmayr, and M. Weidemüller, Phys. Rev. Lett. **100**, 253001 (2008).

[14] T. A. Johnson, E. Urban, T. Henage, L. Isenhower, D. D. Yavuz, T. G. Walker, and M. Saffman, Phys. Rev. Lett. **100**, 113003 (2008).

[15] Y. O. Dudin, L. Li, F. Bariani, and A. Kuzmich, Nature Physics **8**, 790 (2012).

[16] O. Kittelmann, J. Ringling, A. Nazarkin, G. Korn, and I. V. Hertel, Phys. Rev. Lett. **76**, 2682 (1996).

[17] T. Rickes, L. P. Yatsenko, S. Steuerwald, T. Halfmann, B. W. Shore, N. V. Vitanov, and K. Bergmann, The Journal of Chemical Physics **113**, 534 (2000).

[18] S. Lee, J. Lim, J. Ahn, V. Hakobyan, and S. Guérin, Phys. Rev. A **82**, 023408 (2010).

[19] C. Trallero-Herrero, J. L. Cohen, and T. Weinacht, Phys. Rev. Lett. **96**, 063603 (2006).

[20] N. Dudovich, T. Polack, A. Pe'er, and Y. Silberberg, Phys. Rev. Lett. **94**, 083002 (2005).

[21] A. Monmayrant, B. Chatel, and B. Girard, Phys. Rev. Lett. **96**, 103002 (2006).

[22] T. Morishita and C. D. Lin, Phys. Rev. A **87**, 063405 (2013).

[23] M. F. Ciappina, J. A. Pérez-Hernández, A. S. Landsman, T. Zimmermann, M. Lewenstein, L. Roso, and F. Krausz, Phys. Rev. Lett. **114**, 143902 (2015).

[24] S. Hughes, Phys. Rev. Lett. **81**, 3363 (1998).

[25] O. D. Mücke, T. Tritschler, M. Wegener, U. Morgner, and F. X. Kärtner, Phys. Rev. Lett. **87**, 057401 (2001).

[26] K. J. Schafer, in *Strong Field Laser Physics*, edited by T. Brabec (Springer, New York, 2008) p. 111.

[27] M. Ruggenthaler and D. Bauer, Phys. Rev. Lett. **102**, 233001 (2009).

[28] J. I. Fuks, N. Helbig, I. V. Tokatly, and A. Rubio, Phys. Rev. B **84**, 075107 (2011).

[29] J. I. Fuks, M. Farzanehpour, I. V. Tokatly, H. Appel, S. Kurth, and A. Rubio, Phys. Rev. A **88**, 062512 (2013).

[30] J. B. Krieger, Y. Li, and G. J. Iafrate, Phys. Rev. A **45**, 101 (1992).

[31] X.-M. Tong and S.-I. Chu, Phys. Rev. A **57**, 452 (1998).

[32] J. P. Perdew and A. Zunger, Phys. Rev. B **23**, 5048 (1981).

[33] C. A. Ullrich, U. J. Gossmann, and E. K. U. Gross, Phys. Rev. Lett. **74**, 872 (1995).

[34] X.-M. Tong and S.-I. Chu, Phys. Rev. A **55**, 3406 (1997).

[35] S.-I. Chu, J. Chem. Phys. **123**, 062207 (2005).

[36] M. Thiele, E. K. U. Gross, and S. Kümmel, Phys. Rev. Lett. **100**, 153004 (2008).

[37] D. A. Telnov, J. T. Heslar, and S.-I. Chu, Chem. Phys. **391**, 88 (2011).

[38] M. Anwar-ul Haq, S. Mahmood, M. Riaz, R. Ali, and M. A. Baig, J. Phys. B **38**, S77 (2005).

[39] M. E. Casida, in *Recent Advances in Density Functional Methods, Part I*, edited by D. P. Chong (World Scientific, Singapore, 1995) p. 155.

[40] M. Petersilka, U. J. Gossmann, and E. K. U. Gross, Phys. Rev. Lett. **76**, 1212 (1996).

[41] M. S. Safronova, U. I. Safronova, and C. W. Clark, Phys. Rev. A **86**, 042505 (2012).

[42] L. J. Radziemski, R. Engleman Jr, and J. W. Brault, Phys. Rev. A **52**, 4462 (1995).

[43] J. Heslar, D. A. Telnov, and S.-I. Chu, Phys. Rev. A **87**, 052513 (2013).

[44] D. A. Telnov, K. E. Sosnova, E. Rozenbaum, and S.-I. Chu, Phys. Rev. A **87**, 053406 (2013).

[45] J. Heslar, D. A. Telnov, and S.-I. Chu, Phys. Rev. A **91**, 023420 (2015).

[46] L. D. Landau and E. M. Lifshitz, *The classical theory of fields* (Pergamon Press, Oxford, 1975).

[47] G. Vignale, Phys. Rev. Lett. **74**, 3233 (1995).

[48] M. Mundt, S. Kümmel, R. van Leeuwen, and P.-G. Reinhard, Phys. Rev. A **75**, 050501 (2007).

[49] K. Rzazewski and M. Florjanczyk, J. Phys. B **17**, L509 (1984).

[50] D. Roguś and M. Lewenstein, J. Phys. B **19**, 3051 (1986).

[51] K. Rzazewski, J. Zakrzewski, M. Lewenstein, and J. W. Haus, Phys. Rev. A **31**, 2995 (1985).

[52] A. K. Kazansky and D. A. Telnov, Sov. Phys. - JETP **67**, 253 (1988).

[53] D. A. Telnov and S.-I. Chu, J. Phys. B **28**, 2407 (1995).

[54] T.-S. Ho and S.-I. Chu, Chem. Phys. Lett. **141**, 315 (1987).

[55] A. G. Fainshtein, N. L. Manakov, V. D. Ovsiannikov, and L. P. Rapoport, Phys. Rep. **210**, 111 (1992).